Available online at www.sciencedirect.com
ScienceDirect
Trans. Nonferrous Met. Soc. China 35(2025) 1381−1393
Transactions of Nonferrous Metals Society of China
www.tnmsc.cn

Microstructure, mechanical properties, and formability of 1030B Al strip manufactured by ultrasound-assisted continuous casting direct rolling

Li ZHANG[1], Xiao-qian LI[2], Shang GE[1], Guan HUANG[1], Ri-peng JIANG[2], Jing-pei XIE[3], Shao-kang GUAN[1]

1. Henan Province Key Laboratory of Advanced Light Alloys, School of Materials Science and Engineering, Zhengzhou University, Zhengzhou 450001, China;
2. Light Alloy Research Institute, Central South University, Changsha 410083, China;
3. School of Materials Science and Technology, Henan University of Science and Technology, Luoyang 471003, China

Received 8 September 2023; accepted 20 June 2024

Abstract: The microstructure and properties of a 1030B Al strip were improved by applying ultrasonic melt treatment (UMT) in a Hazelett continuous casting direct rolling production line. The microstructure and properties of the 1030B Al strip were investigated by scanning electron microscopy, electron backscatter diffraction, and tensile testing. Applying UMT reduced the average grain size of the as-cast sheet by more than 28.0% with respect to that of the normal samples without UMT. When UMT was applied, the rolled strip inherited the refined grains from the as-cast sheet with an average grain size smaller than 63.0 μm. Meanwhile, the dislocation density was increased by the grain refinement, dynamic recovery, and recrystallization during rolling. Accordingly, the strain-hardening rates of the rolled samples after UMT were generally higher than those of the normal samples, and the strength of the rolled strip was also improved. Furthermore, the rolled strip exhibited better formability with higher strain-hardening exponents and Erichsen index values.

Key words: grain refinement; mechanical properties; formability; continuous casting direct rolling; ultrasonic melt treatment; 1030B Al

1 Introduction

Given the increasing demand to decrease carbon emissions and to develop green processes in the aluminum industry, near-net-shape technology has attracted increasing attention worldwide. With this technique, the billet is cast with a thickness as close as possible to that of the final product, which increases productivity and reduces resource consumption and waste emissions [1]. Thus, continuous cast rolling (CCR) or twin-roll casting (TRC) is gradually replacing breakdown hot rolling in the manufacturing of Al alloys that cannot be strengthened by heat treatment [2−4]. Moreover, the stand-alone output of continuous casting direct rolling (CCDR) is considerably higher than that of CCR or TRC, and the range of alloys that can be produced by CCDR has expanded considerably [5]. Therefore, the CCDR process has tremendous potential for the production of wide Al sheets (1320−2300 mm) for foils (1xxx, 3xxx, 4xxx, 5xxx, and 8xxx Al alloys), which are extensively used in ships, air conditioners, and batteries [6,7]. However, unlike steel plates produced by CCDR, the as-cast Al slab from the continuous casting machine is rolled directly by using its residual heat without homogenization [8]. Consequently, the final

Corresponding author: Li ZHANG, Tel: +86-13373956611, E-mail: zhanglicsu@zzu.edu.cn;
Shao-kang GUAN, E-mail: skguan@zzu.edu.cn
https://doi.org/10.1016/S1003-6326(24)66755-5

rolled strip inherits casting defects such as coarse grains, solute segregation, and the agglomeration of intermetallics, which severely deteriorates its mechanical properties and formability. Therefore, technological innovations, especially in the continuous casting stage, may improve the quality of the final Al strip prepared via CCDR.

Al melt treatment during the continuous casting stage is an effective method for suppressing or eliminating microstructural defects from the original slab. Owing to the large flux in a single Al melt input, the launder and conticaster used in CCDR are longer than those used in CCR or TRC, thus increasing the difficulty of the melt treatment. Typically, the addition of grain refiners, such as Al−Ti−B, and the application of physical fields, such as electromagnetic and ultrasonic fields, positively affect the melt solidification process [9−11]. Among these methods, ultrasonic melt treatment (UMT) is the easiest to implement in the CCDR production line because of its adjustability and mobility [12,13]. By taking advantage of the nonlinear effects, namely cavitation and acoustic streaming, generated by ultrasonic waves in an Al melt, UMT has been successfully utilized in the TRC process [14,15]. The application of ultrasound with a power of 300 W and incident angle of 45° in the roll casting of 1235 Al strips significantly refined the grains [16]. In addition, the observable centerline segregation and clear macroscale edge cracks in a conventional TRC 1050 Al strip were effectively suppressed by acoustic streaming and the microjets caused by the collapse of cavitation bubbles [15]. Similar effects were observed in ultrasound-assisted TRC Mg-alloy strips; specifically, the α-Mg grains were refined, and the intermetallic $Mg_{17}(Al,Zn)_{12}$ and MgAlCeMn phases were modified for the Mg−3wt.%Al−1%Zn−0.8%Ce−0.3%Mn alloy during the ultrasound-assisted TRC process [17]. In addition, UMT reduced the anisotropy of a TRC AZ31B strip, and its mechanical properties were improved owing to the refined grains and uniform microstructure produced by UMT [18].

In the present study, a multiple-stage UMT method was applied at key positions in a Hazelett CCDR strip production line according to the melt flow rate and volume. Based on the experimental results, the effects of UMT on the microstructure, mechanical properties, and formability of the CCDR strip were investigated. The corresponding mechanisms underlying the improvements in the microstructure and properties of the strip were also examined.

2 Experimental

2.1 Ultrasound-assisted Hazelett CCDR process

Schematic and field-test images of the ultrasound-assisted Hazelett CCDR process are shown in Fig. 1. The twin-belt caster was internally cooled by water at temperatures of 25−30 °C and at a flow rate of 16.5 L/min. The UMT system included a power-supply box and an ultrasonic rod with a titanium sonotrode (50 mm in diameter) driven by an air-cooled piezoelectric transducer (~20 kHz) at a working power of 2 kW (corresponding to a 20 μm peak-to-peak amplitude). First, the ultrasonic generators were turned on to make the sonotrodes resonate in the air, and then, the ultrasonic system was adjusted immediately after immersing the sonotrodes into the Al melt to ensure that it reached a steady state. In contrast with

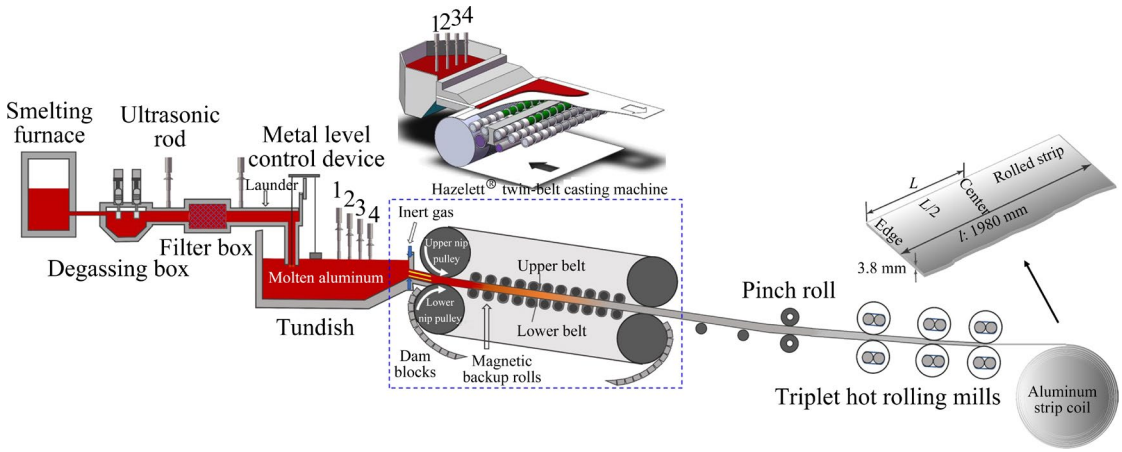

Fig. 1 Schematic of UMT-assisted Hazelett CCDR process

a previous study [12], the insertion depth gradient of the sonotrodes in the tundish was varied, with insertion depths of 150 mm for the outer two sonotrodes (#1 and #4) and 50 mm for the middle two sonotrodes (#2 and #3). This was intended to broaden the ultrasonic effect on the Al melt for different liquid levels in the tundish. During continuous casting, the Al−Ti−B refiner wire was automatically fed into the Al melt with amount of 0.2 wt% (2 kg/10^3 kg Al) at the outlet of the smelting furnace. The as-cast sheet (without homogenization) was then delivered into the rolling mills by a pinch roll after the recirculation of the cooling water spray. During rolling, the rollers were cold, and the as-cast sheet was rolled utilizing its own residual heat. After three rolling passes, the rolled strip was curled into coils. The dimension of the as-cast billet was 1980 mm (width) × 19 mm (thickness), and that of the rolled strip was 1980 mm (width) × 3.8 mm (thickness). Both had a chemical composition of Al−0.29Fe−0.16Mn−0.14Si−0.05Ti−0.006Zn−0.003Cu−0.001Mg (wt.%).

2.2 Characterization

Figure 2 shows the sampling positions and sample dimensions. For the microstructural observations, squares with dimensions of 10 mm × 10 mm × 3.8 mm were sectioned from the edge, *L*/2, and center of the strips. The samples were then ground, mechanically polished, electropolished, and anodized. The grain structure of the as-cast billet was examined using an optical microscope (OLYMPUS GX51, Japan) under polarized light, while that of the rolled strip was detected using electron backscatter diffraction (EBSD, EVO MA10, Zeiss, Germany) with a step size of 0.9 μm at an accelerating voltage of 15 kV. Tensile testing

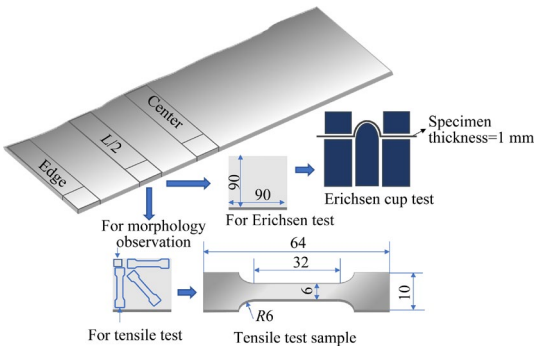

Fig. 2 Schematic showing sampling positions and sample dimensions (unit: mm)

was conducted using an Instron® 3369 mechanical testing machine at the ambient temperature with a loading rate of 1 mm/min. The tensile test samples were cut from strips along the rolling direction (RD), at an orientation of 45° with respect to the RD and along the transverse direction (TD, 90° to the RD). For the formability test, blocks with dimensions of 90 mm × 90 mm × 1 mm were cut and punched using an Erichsen test machine at a speed of 10 mm/min. All tests were repeated at least twice for each strip.

3 Results

3.1 Microstructure

Figure 3 shows the grain structure at representative positions in the as-cast sheet, and Table 1 presents the corresponding average grain size (AGS). Equiaxed grains can be observed in both sheets, whereas the grains in the normal sheet without UMT appear coarser than those in the sheet prepared with UMT. The AGS was approximately 100.0 μm for the normal sheet, with size of (101.2±4.1) μm at the edge, (103.3±5.3) μm at *L*/2, and (98.7±2.9) μm at the center. After UMT, the AGS of the sheet was reduced to approximately 70.0 μm, with the size of (67.8±2.2) μm at the edge, (69.5±1.6) μm at *L*/2, and (70.5±1.9) μm at the center. The grain-refinement efficiencies obtained at these three positions following UMT were calculated to be 33.0%, 32.7% and 28.6%, respectively.

Figure 4 shows the grain morphology and AGS of the rolled strips at the three representative positions with and without UMT. The grains were elongated along the RD in both strips, and some subgrains appeared. At the edges of the two strips, almost all the grains presented the ⟨001⟩ orientation (marked in red) and ⟨101⟩ orientation (marked in green). At *L*/2 of the strips, the number of ⟨001⟩-oriented grains decreased, and some of the grains transformed into the ⟨111⟩ orientation. At the center, most of the grains maintained the ⟨001⟩ and ⟨101⟩ orientations, and these grains appear to have replaced the ⟨111⟩-oriented grains. The grain size distributions (Figs. 4(g−i)) indicate that several coarse grains larger than 100.0 μm were distributed at the edges of both strips. However, at *L*/2 and the center of the UMT strip, the proportion of grains larger than 100.0 μm in the strip was reduced. In

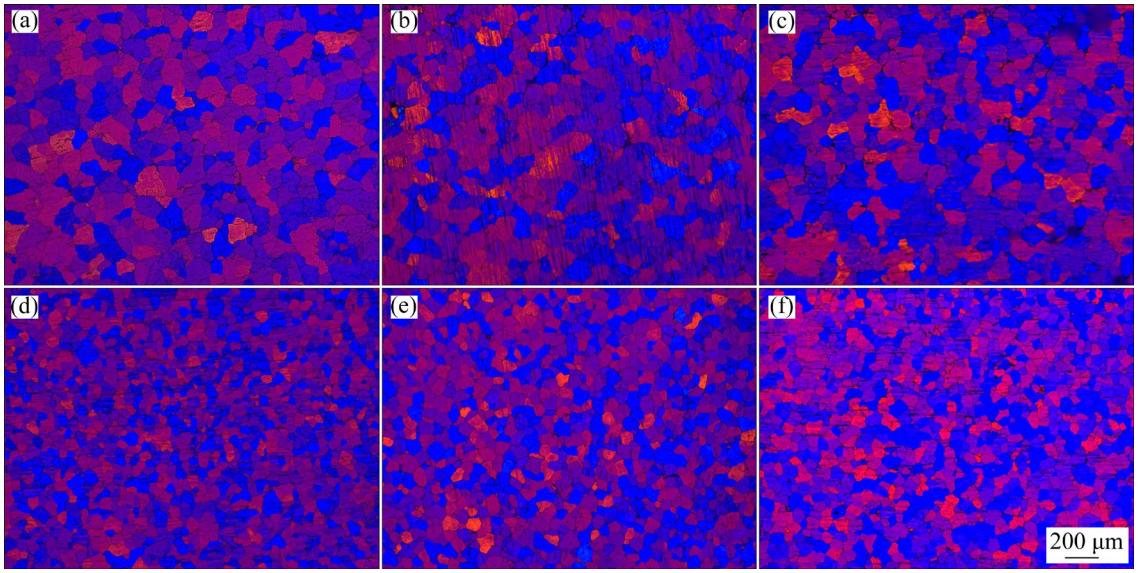

Fig. 3 Grain structures of as-cast samples taken from edge without UMT (a), *L*/2 without UMT (b), center without UMT (c), edge with UMT (d), *L*/2 with UMT (e), and center with UMT (f)

Table 1 AGS of as-cast sample (μm)

Sample	Edge	*L*/2	Center
Without UMT	101.2±4.1	103.3±5.3	98.7±2.9
With UMT	67.8±2.2	69.5±1.6	70.5±1.9

summary, based on the results in Fig. 4, the AGS declined from (69.6±2.4) to (62.2±2.1) μm at the edge, from (66.8±3.2) to (56.1±2.7) μm at *L*/2, and from (61.9±1.9) to (56.7±2.3) μm at the center after UMT, with reduction rates of 10.6%, 16.0% and 8.4%, respectively.

Figure 5 shows the fractions of recrystallization, high-angle grain boundaries (HAGBs), and low-angle grain boundaries (LAGBs) in the rolled samples. Because the as-cast sheet was directly rolled using only its residual heat, and the rolled strip was not heat-treated, dynamic recovery (DRV) tended to occur in Al that possessed a high stacking fault energy [19]. Furthermore, the elongated deformed grains with a small number of subgrains indicated the occurrence of dynamic recrystallization (DRX) during rolling. Figure 5(b) shows that more than 60% of the grain boundaries in the rolled samples were LAGBs, irrespective of whether UMT was used, thus indicating limited DRX during the rolling process [20]. This finding is consistent with the fact that deformed structures and substructures dominate the rolled samples. By contrast, the rolled samples that underwent UMT contained somewhat more subgrains, which explains why the AGS was relatively small in these samples.

Figure 6 illustrates the kernel average misorientation (KAM) diagrams and corresponding KAM values. The average KAM values for the rolled samples subjected to UMT were marginally higher than those of the samples without UMT. In addition, the KAM value for the sample at *L*/2 without UMT was the lowest among those of all samples. This indicates that the UMT samples contained more dislocations in the matrix than the normal samples, which may have promoted strain hardening during plastic deformation [21].

3.2 Mechanical properties and formability

Figure 7 depicts the true stress–strain curves recorded from the rolled strip samples during tensile testing. The curves indicate that the ultimate tensile strength (UTS) of the samples along the RD (Fig. 7(a)) and TD (Fig. 7(c)) were generally higher than that along the 45° direction (Fig. 7(b)). In addition, for both rolled strips, the UTS of the samples taken from the center were higher than those of the edge and *L*/2 samples.

Figure 8 shows the strain-hardening rate curves, which demonstrates that the strain-hardening rates for the samples after UMT at the initial stage were generally higher than those for the normal samples in all directions, except for the samples taken from the center along the RD and at 45°. In addition, the strain-hardening rates of the

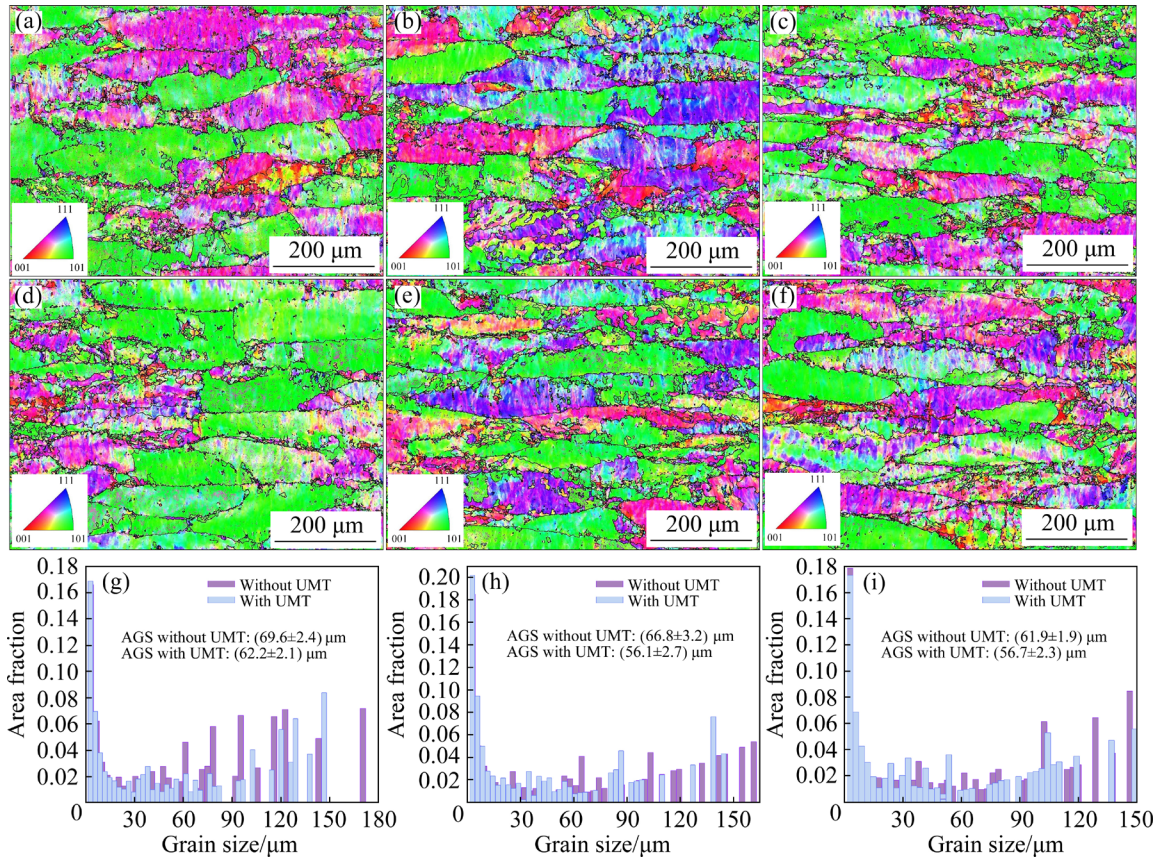

Fig. 4 Grain morphology of rolled samples taken from edge without UMT (a), *L*/2 without UMT (b), center without UMT (c), edge with UMT (d), *L*/2 with UMT (e) and center with UMT (f), and corresponding grain-size distributions and AGS at edge (g), at *L*/2 (h) and at center (i)

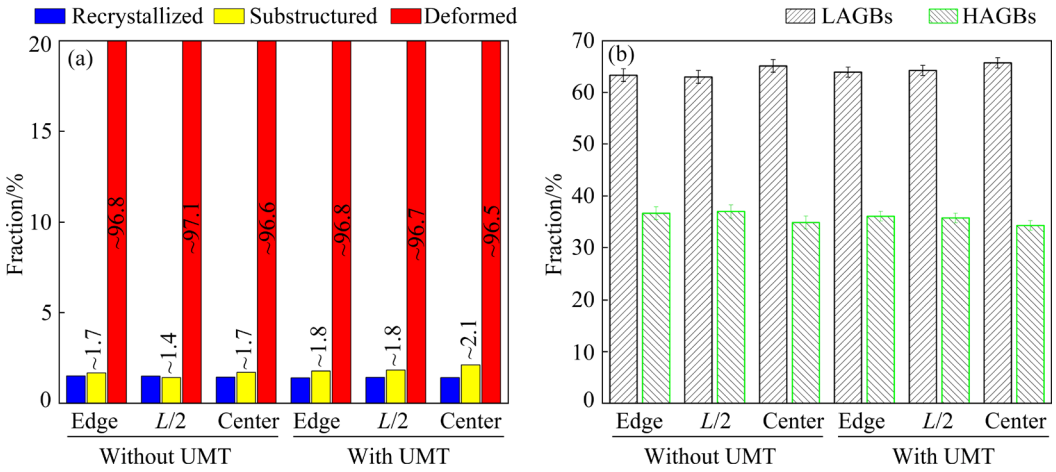

Fig. 5 Fractions of recrystallized grains (a) and HAGBs and LAGBs (b) of rolled samples

samples along the RD were marginally higher, and the rate decreased most rapidly along the direction oriented at 45°, followed by those along the TD and then the RD.

The strain-hardening behavior of the samples was defined using the Hollomon equation [21]:

$$\sigma=k\varepsilon^{n} \quad (1)$$

where σ, ε, k and n represent the true stress, true strain, strength coefficient and stain-hardening exponent, respectively. The strain-hardening exponent, n, can be obtained from the slope of the logarithmic form of Eq. (1) via linear regression fitting:

$$\ln\sigma=\ln k+n\ln\varepsilon \quad (2)$$

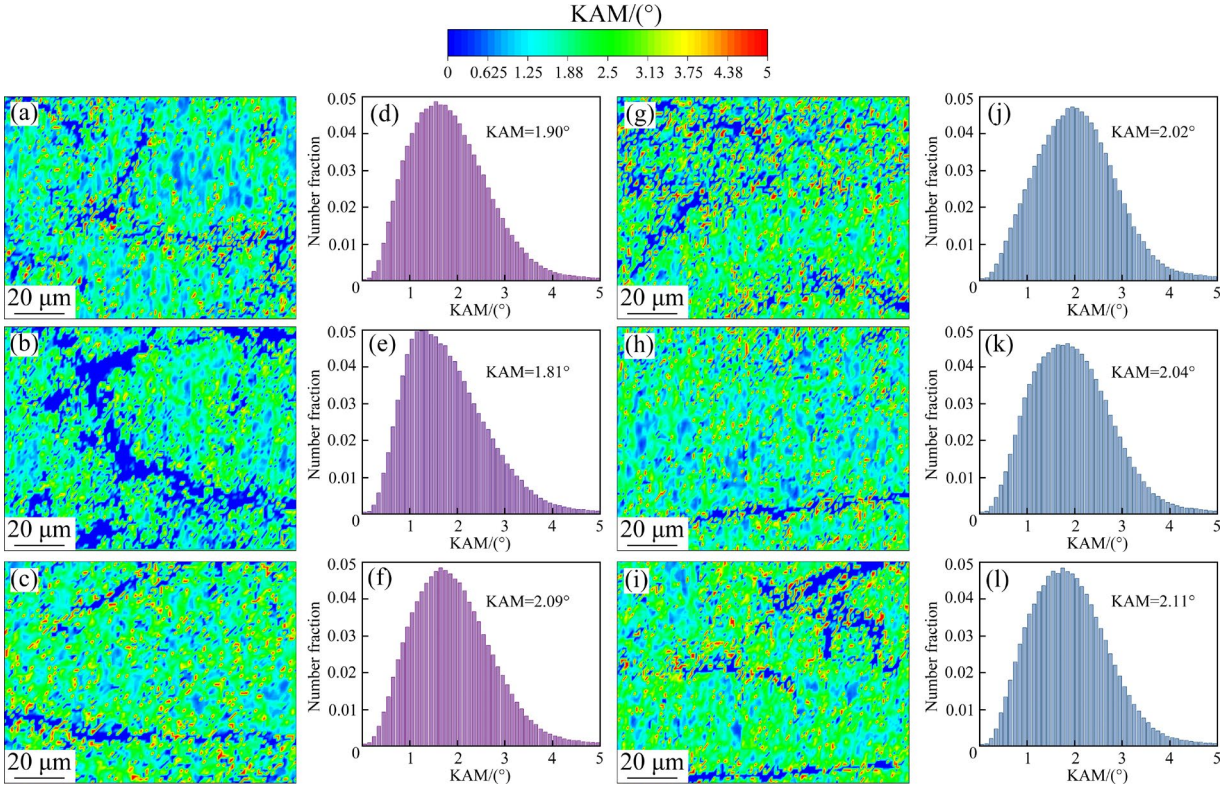

Fig. 6 KAM maps of rolled samples taken from edge without UMT (a), *L*/2 without UMT (b), center without UMT (c), edge with UMT (g), *L*/2 with UMT (h) and center with UMT (i), and corresponding KAM values without UMT (d−f) and with UMT (j−l)

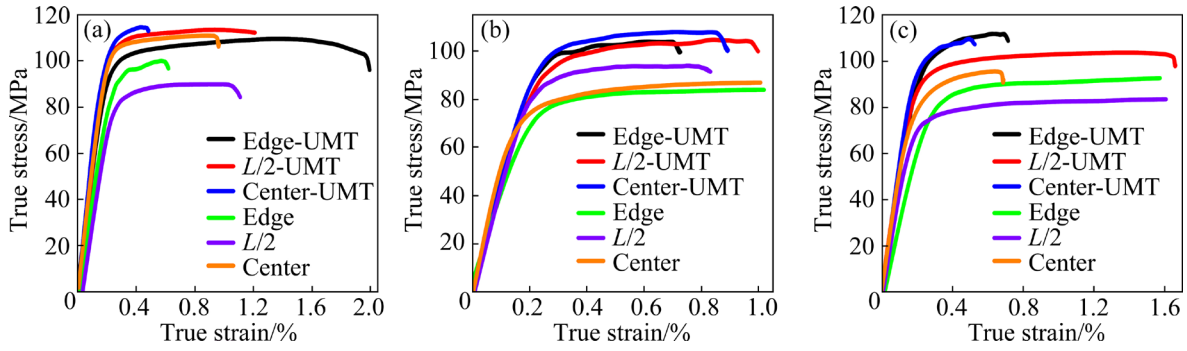

Fig. 7 True stress–strain curves of rolled samples: (a) Along RD; (b) Along direction oriented at 45°; (c) Along TD

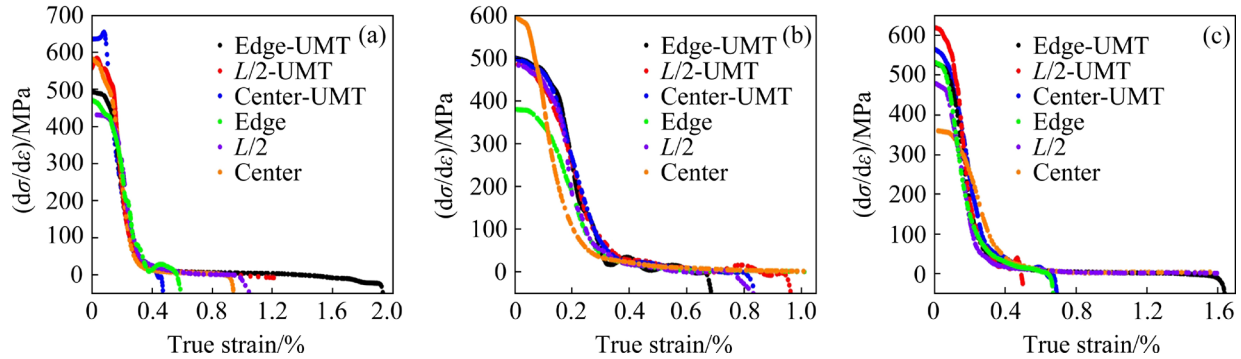

Fig. 8 Strain-hardening rate (dσ/dε) curves of rolled samples: (a) Along RD; (b) Along direction oriented at 45°; (c) Along TD

$$n=\frac{\mathrm{d}\ln\sigma}{\mathrm{d}\ln\varepsilon} \tag{3}$$

Thus, based on the values of σ and ε in the uniform plastic-deformation stage in the true stress–strain curves, the n values of the samples were determined from the fitted $\ln\sigma-\ln\varepsilon$ curves.

Table 2 summarizes the UTS, yield strength (YS), elongation (EL) and n values of the rolled samples obtained from different positions and directions with and without UMT. After UMT, the UTS and YS increased to values of >105 MPa and >90 MPa, respectively, showing the greatest improvement along the RD and TD. The EL values did not change in the cases of the samples obtained along the TD at all three positions. However, UMT improved the EL values of the samples cut from the $L/2$ and center regions along the RD and the samples obtained at $L/2$ along the 45° direction. Along the RD, UMT increased the UTS and YS by 9.5% and 15.8% at the edge, by 26.1% and 42.3% at $L/2$, and by 3.2% and 2.3% at the center after UMT, respectively. The average n values of the samples obtained at the edge, $L/2$, and center of the two strips were calculated using the relation of $n_{\text{average}}=(n_{\text{RD}}+2n_{45°}+n_{\text{TD}})/4$ [22]. The n_{average} values were higher for the UMT strip than for the normal strip and gradually decreased from the edge to the center for both strips. At the edge and $L/2$, the n values increased after UMT in the samples taken along the same direction, except for the sample cut from the edge along RD. However, UMT increased the average n values for the samples obtained at all representative positions, thus indicating improved uniform plastic-deformation ability [23].

Figure 9 shows the fracture morphologies of the tensile samples, wherein typical plastic-fracture characteristics can be observed. However, the fracture surfaces of the samples after UMT were smoother than those of the normal samples. In addition, the dimples were smaller and distributed more uniformly in the UMT samples, whereas shrinkage occurred in the normal samples. The defects generated during casting were likely inherited by the rolled strips during the conventional CCDR process.

Table 2 UTS, YS, EL and n values of rolled samples obtained at different positions and directions without and with UMT

Sample	Direction	UTS/MPa	YS /MPa	EL/%	n	n_{average}
Edge-UMT	RD	109.6±2.2	87.3±1.6	4.6±0.2	0.098±0.012	0.138
	45°	103.9±2.7	83.4±1.5	2.7±0.3	0.153±0.020	
	TD	111.9±2.6	87.4±1.6	3.2±0.2	0.146±0.018	
Edge	RD	100.1±3.2	75.4±2.6	2.8±0.3	0.131±0.019	0.107
	45°	83.9±2.1	69.1±2.5	4.2±0.2	0.081±0.011	
	TD	92.7±2.2	64.6±2.6	3.5±0.3	0.133±0.017	
$L/2$-UMT	RD	113.5±1.7	94.9±0.8	3.4±0.2	0.134±0.017	0.113
	45°	104.7±1.8	81.6±0.9	4.4±0.3	0.120±0.015	
	TD	103.7±1.7	85.8±0.9	3.7±0.3	0.077±0.009	
$L/2$	RD	90.0±2.7	66.7±1.5	3.1±0.4	0.087±0.009	0.090
	45°	93.9±2.4	77.6±1.5	3.0±0.3	0.101±0.011	
	TD	83.5±2.4	68.8±1.6	3.6±0.4	0.069±0.007	
Center-UMT	RD	114.7±3.1	97.9±0.9	2.8±0.3	0.143±0.012	0.096
	45°	107.9±2.8	85.0±0.8	3.9±0.2	0.080±0.007	
	TD	109.6±2.9	92.3±0.8	2.8±0.3	0.082±0.007	
Center	RD	111.1±4.1	95.7±1.8	3.1±0.4	0.063±0.006	0.093
	45°	86.9±3.2	73.4±1.9	4.1±0.4	0.105±0.010	
	TD	95.6±3.1	77.5±1.8	2.9±0.3	0.098±0.010	

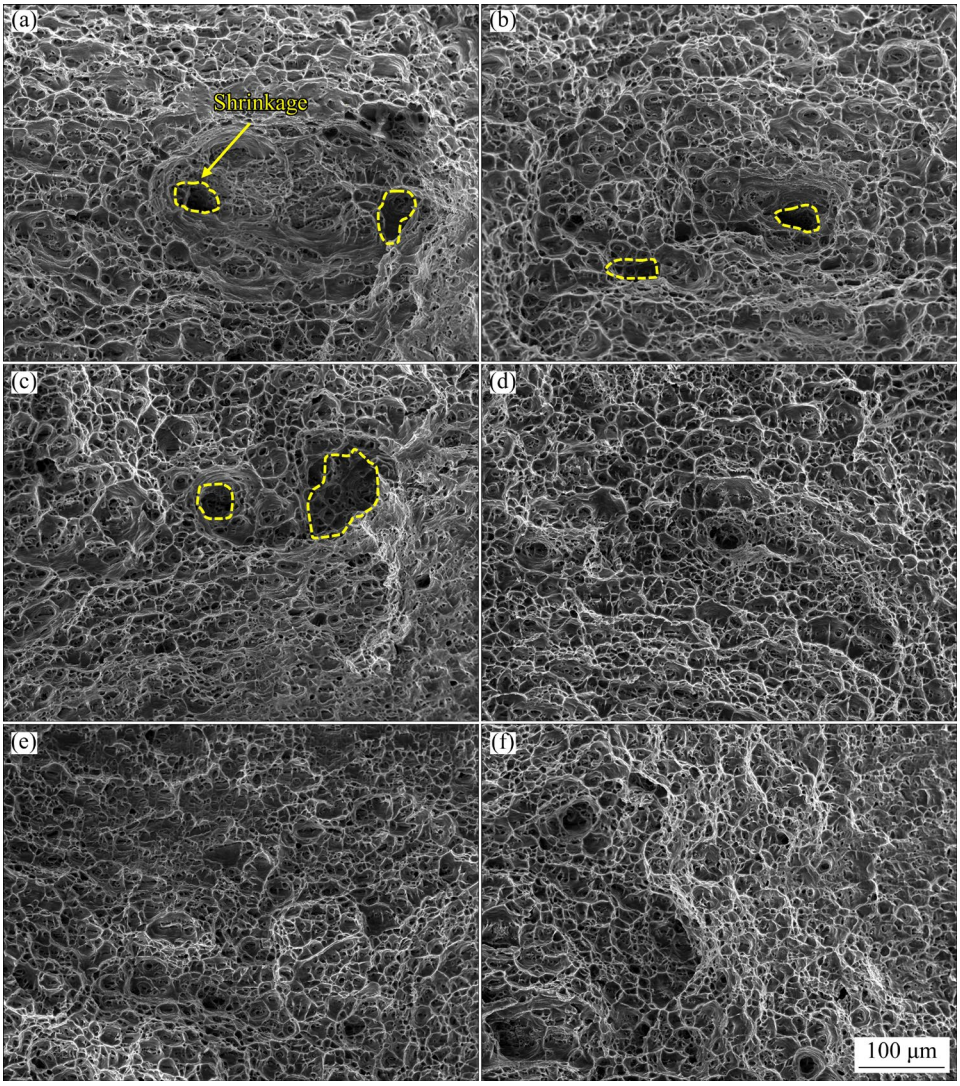

Fig. 9 Fracture morphologies of tensile samples taken from edge without UMT (a), *L*/2 without UMT (b), center without UMT (c), edge with UMT (d), *L*/2 with UMT (e) and center with UMT (f)

Figure 10 shows the cupping curves and macrophotographs of the samples after the Erichsen tests. For the normal samples, the Erichsen index (IE) values at room temperature were lower than 9.0 mm, with values of (7.5±0.1), (8.3±0.2), and (8.5±0.3) mm for the samples obtained from the edge, *L*/2, and center, respectively. After UMT, the corresponding IE values increased to more than 9.0 mm, with values of (9.0±0.3) mm at the edge, (9.4±0.2) mm at *L*/2, and (9.1±0.2) mm at the center.

4 Discussion

4.1 Effect of UMT on grain size

The aforementioned results indicate that UMT positively affected the microstructure, mechanical properties, and formability of the CCDR strip. In the present study, UMT was simultaneously applied in the launder and tundish. When ultrasound propagates in the Al melt, nonlinear effects, such as cavitation and acoustic streaming are generated, which influence nucleation and solute diffusion [14,24,25]. Cavitation bubbles typically form, grow, and collapse during the alternation of negative and positive acoustic pressures as the ultrasound propagates. Local high temperatures (>5000 K), high-energy shock waves exceeding 1000 MPa, and microjets with speeds of approximately 100 m/s are generated at the time of the collapse [26,27]. In this case, mass transfer was accelerated, and the agglomerated Al−Ti−B clusters could be broken down under UMT conditions. Indeed, the Al−Ti−B refiner in our previous study was distributed more

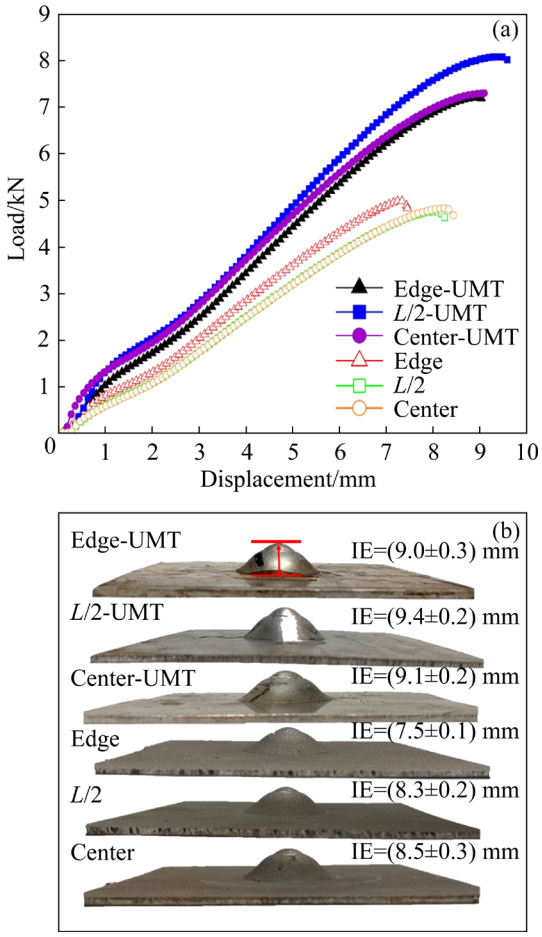

Fig. 10 Cupping curves (a) and macrophotographs (b) of samples after Erichsen test

uniformly after UMT, and a higher Ti content was detected at the outlet of the filter box and tundish [12]. This was probably because agglomerated Al−Ti−B clusters were scattered by UMT, allowing more dispersed Al−Ti−B particles to pass successfully through the filter box and enter the tundish. Subsequently, four-source UMT in the tundish would fully stir the Al melt therein, thereby dispersing the solutes and Al−Ti−B refiners.

The minimum acoustic pressure that causes the cavitation effect is called the cavitation threshold of the liquid [28]. According to the formula of $I=1/2\rho c(2\pi fA)^2$ [29], the acoustic intensity is calculated to be 1994 W/cm^2 in the current study, which is much higher than the theoretical cavitation threshold (100 W/cm^2 in the Al melt) required to produce cavitation in the Al melt [29]. For values higher than the cavitation threshold under UMT conditions, the relationship between the number of nucleation sites and grain size can be expressed as follows [30]:

$$D_{gs}=5.6\frac{Dz\Delta T_n}{vQ}+\frac{1}{\sqrt[3]{f(A)N_v}} \quad (4)$$

where D_{gs} is the grain size, D is the diffusion coefficient of the solute atoms, $z\Delta T_n$ is the additional undercooling required to stimulate the next nucleation, v is the growth rate of α-Al grains, Q is the growth restriction factor of the grains, f is the fraction of heterogeneous particles required to successfully nucleate a grain, A is the ultrasound amplitude, and N_v is the number density of heterogeneous particles in the Al melt. This formula indicates that if other parameters (including the ultrasound amplitude) are the same above the cavitation threshold, the grain size is mainly determined by the number density of heterogeneous particles in the Al melt. Thus, as the Al melt with more dispersed Al_3Ti/TiB_2 particles flowed into the caster from the nozzle, the heterogeneous nucleation rate of α-Al increased, thus refining the grains of the as-cast billet. This also indicates that the utilization rate of the added refiners can be increased by UMT during industry-level casting processes.

Subsequently, most of the grains were elongated and turned into deformed structures during three rounds of continuous rolling. The refined grains in the UMT billet possessed greater deformation resistance during rolling, and the extent of grain deformation was not as large as that in the normal rolled samples, which narrowed the difference in the grain size between the rolled strips with and without UMT. Conversely, DRV and DRX occurred during rolling, which increased the amount of subgrains and reduced the grain sizes of the UMT rolled samples. However, DRX was not significant; thus, it did not contribute considerably to the grain-size reduction in the UMT rolled samples.

4.2 Effect of UMT on mechanical properties and formability

In the present study, the UTS and YS of the rolled strips were improved after UMT. Fine-grain strengthening and dislocation strengthening were the primary strengthening mechanisms because neither a precipitation phase nor a solid solution formed during the cold rolling of commercial-purity Al. The relationship between the YS and grain size can be described by the Hall–Petch equation as follows [31,32]:

$$\Delta\sigma_{\text{grain}}=k\left(\frac{1}{\sqrt{d_{\text{UMT}}}}-\frac{1}{\sqrt{d_{\text{n}}}}\right) \quad (5)$$

where k is the corresponding strengthening coefficient (68 MPa·μm$^{1/2}$ for Al) [33], and d_{UMT} and d_{n} are the AGS values of the rolled samples with and without UMT, respectively. Because of the small difference in these two AGS values, this calculation confirmed that grain refinement did not contribute significantly to the strength, which was within 1 MPa.

In addition, LAGBs dominated in both types of rolled strips, and the dislocation density was slightly higher in the samples that underwent UMT, as evidenced by the results in Figs. 5 and 6. Additionally, the formation of subgrains by DRV and DRX during rolling would lead to the continuous movement and convergence of dislocations in LAGBs. In this case, the lattice slip was hindered by dislocation interactions between subgrains, recrystallized grains, and deformed grains, and greater forces were required to plastically deform the alloy, which increased the YS. The contribution of dislocation strengthening could be calculated using the following Bailey−Hirsch formula [34,35]:

$$\Delta\sigma_{\text{dislocation}}=M\alpha Gb(\sqrt{\rho_{\text{UMT}}}-\sqrt{\rho_{\text{n}}}) \quad (6)$$

where M is the Taylor factor; α is a constant between 0.2 and 0.5 (0.2 for Al) [36]; G is the shear modulus, which is typically equal to 26.9 GPa for Al [37]; b is the magnitude of Burgers vector (0.286 nm) [37]; and ρ_{UMT} and ρ_{n} are the dislocation density values for the UMT and normal samples, respectively, which can be calculated from the average KAM value [38,39].

$$\rho=\frac{2\overline{\text{KAM}}}{l_{\text{ss}}b} \quad (7)$$

where $\overline{\text{KAM}}$ is the average KAM value, which can be obtained from Fig. 6, and l_{ss}=0.9 μm is the scan step length for EBSD. The ρ_{n} values at the edge, L/2, and center, were calculated to be 1.48×10^{16}, 1.41×10^{16}, and 1.62×10^{16} m^{-2}, respectively, and the corresponding ρ_{UMT} values were calculated to be 1.57×10^{16}, 1.59×10^{16}, and 1.64×10^{16} m^{-2}.

Subsequently, the predicted YS ($\sigma_{\text{predicted}}$) was calculated as follows [40]:

$$\sigma_{\text{predicted}}=\Delta\sigma_{\text{grain}}+\Delta\sigma_{\text{dislocation}}+\Delta\sigma_{\text{n}} \quad (8)$$

where σ_{n} (64.6 MPa) is the YS of the normal samples without UMT. Using the primary parameters from Eqs. (5)−(8), the contributions of grain refinement and dislocation strengthening to the increase in the YS for the UMT sample obtained at L/2 along the RD were calculated to be 0.8 MPa and 33.0 MPa, respectively. In addition, the YS value (98.4 MPa) predicted by Eq. (8) was close to the measured value (94.9 MPa), confirming that dislocation strengthening played the dominant role among the two strengthening mechanisms.

Typically, the strength increases at the expense of plasticity. However, in the present study, not only the strength but also the ductility and formability improved in the rolled strip after UMT. The higher n values of the strip after UMT indicated a lower sensitivity to strain localization, which implied better EL and ductility of the strip [41]. This was mainly attributed to the grain refinement with UMT, which increased the number of grains per unit volume. Under the same deformation conditions, more grains were involved in the deformation, thereby increasing the deformation uniformity, mitigating the formation and expansion of cracks, and enabling larger plastic deformation before fracture [42]. In summary, UMT directly affected the nucleation of the α-Al grains during casting, with hereditary effects on the grain structure and properties of the rolled strip. The results of the present study also indicate that a front-end melt treatment is an effective method for simultaneously improving the microstructure, mechanical properties, and formability of Al strips during near-net-shape manufacturing.

5 Conclusions

(1) The α-Al grains were significantly refined by ultrasound-assisted solidification to sizes smaller than 70 μm, with grain-refining efficiencies of 33.0% at the edge, 32.7% at L/2, and 28.6% at the center. The rolled strip inherited the refined grain structure of the as-cast UMT billet, and the AGS was reduced to be <63 μm, representing a decrease of more than 8% with respect to that of the normal strip.

(2) The strength of the rolled strip was improved after UMT. The UTS and YS were increased to be >105 and >90 MPa after UMT, respectively, especially for the samples taken along

the RD and TD, with the largest increase of 26.1% in the UTS and 42.3% in the YS observed at *L*/2. A theoretical analysis showed that the main contribution to the increment in the YS case was dislocation strengthening.

(3) The EL values were improved for the samples obtained at *L*/2 and the center along RD, and for the samples at *L*/2 in the 45° direction after UMT. The IE values of the UMT strip increased to be >9.0 mm, and the average strain-hardening exponent (*n*) values for the UMT strip were higher than those for the normal strip.

CRediT authorship contribution statement

Li ZHANG: Writing − Original draft, Data curation, Investigation, Methodology, Funding acquisition; **Xiao-qian LI:** Supervision, Project administration, Resources; **Shang GE** and **Guan HUANG:** Data curation, Formal analysis; **Ri-peng JIANG:** Investigation, Writing − Review & editing; **Jing-pei XIE:** Investigation, Resources; **Shao-kang GUAN:** Supervision, Project administration, Funding acquisition.

Declaration of competing interest

The authors declare that they have no known competing financial interests or personal relationships that could have appeared to influence the work reported in this paper.

Acknowledgments

The authors would like to acknowledge the National Natural Science Foundation of China (No. 52004254), and the Major Science and Technology Project of Henan Province, China (No. 221100240300). Technicians at Luoyang Longding Aluminum Industries Co., Ltd. (China) are thanked for Providing Experimental Assistance.

References

[1] KLINKENBERG C, KINTSCHER B, HOEN K, REIFFERSCHEID M. More than 25 years of experience in thin slab casting and rolling current state of the art and future developments [J]. Steel Research International, 2017, 88(10): 1700272.

[2] HAGA T, TKAHASHI K, IKAWAAND M, WATARI H. Twin roll casting of aluminum alloy strips [J]. Journal of Materials Processing Technology, 2004, 153: 42−47.

[3] LI B Q. Producing thin strips by twin-roll casting: Part I. Process aspects and quality issues [J]. JOM, 1995, 47: 29−33.

[4] LEE Y S, KIM H W, CHO J H. Process parameters and roll separation force in horizontal twin roll casting of aluminum alloys [J]. Journal of Materials Processing Technology, 2015, 218: 48−56.

[5] KASE M, MATSUZUKA K, TAKAHASHI H, OBA H, HIRATA O. Continuous casting direct rolling technology at Nippon Steel's Sakai Works [J]. Steel Times, 1985, 213(6): 268.

[6] HUANG Bo-chin, CHANG Kai-chieh, HUNG Fei-yi. Study on microstructure, mechanical properties and erosion characteristics of Al−Si alloy manufactured by continuous casting direct rolling process [J]. Applied Sciences, 2021, 11(18): 8351.

[7] HUANG Bo-chin, HUNG Fei-yi. Effect of tensile loading−unloading cyclic plastic deformation on 4043 aluminum alloy manufactured through CCDR [J]. Materials Today Communications, 2023, 34: 104979.

[8] ZHAO Jun-ren, HUNG Fei-yi, CHEN Bo-jou. Effects of heat treatment on a novel continuous casting direct rolling 6056 aluminum alloy: Cold rolling characteristics and tensile fracture properties [J]. Journal of Materials Research and Technology, 2021, 11: 535−547.

[9] XIAO Fei, WU Ming-xu, WANG Yi-xiao, ZHOU Wen-zhe, WANG Shu-bin, WANG Dong-hong, ZHU Guo-liang, JIANG M, SHU Da, MI Jia-wei, SUN Bao-de. Effect of trace boron on grain refinement of commercially pure aluminum by Al−5Ti−1B [J]. Transactions of Nonferrous Metals Society of China, 2022, 32(4): 1061−1069.

[10] LÜ Shu-lin, ZHAO Di-jia, JI Xiao-yuan, GUO Wei. Effect of ultrasonic vibration on microstructure and mechanical properties of $Mg_{98}Y_{1.0}Ni_{0.5}Al_{0.5}$ alloy containing LPSO structure [J]. Transactions of Nonferrous Metals Society of China, 2023, 33(1): 59−66.

[11] LUO Lei, XIA Hong-ying, LUO Liang-shun, SU Yan-qing, CAI Chao-jun, WANG Liang, GUO Jing-jie, FU Heng-zhi. Eliminating shrinkage defects and improving mechanical performance of large thin-walled ZL205A alloy castings by coupling travelling magnetic fields with sequential solidification [J]. Transactions of Nonferrous Metals Society of China, 2021, 31(4): 865−877.

[12] JIANG Ri-peng, ZHAO Wen-hao, ZHANG Li, LI Xiao-qian, GUAN Shao- kang. Microstructure and corrosion resistance of commercial purity aluminum sheet manufactured by continuous casting direct rolling after ultrasonic melt pre-treatment [J]. Journal of Materials Research and Technology, 2023, 22: 1522−1532.

[13] ZHANG Li, LI Rui-qing, JIANG Ri-peng, ZHANG Li-hua, LI Xiao-qian. A comparative study on the effect of four-source ultrasonic power on the microstructure and mechanical properties of large-scale 2219 aluminum ingots [J]. JOM, 2019, 71: 2063−2071.

[14] ĖSKIN G I, ESKIN D G. Ultrasonic treatment of light alloy melts [M]. 2nd ed. Boca Raton: CRC Press, 2015.

[15] HUANG Jin-xian, LI Jian-guo, LI Cong, HUANG Chun-fa, FRIEDRICH B. Elimination of edge cracks and centerline segregation of twin-roll cast aluminum strip by ultrasonic melt treatment [J]. Journal of Materials Research and Technology, 2020, 9(3): 5034−5044.

[16] MAO Da-heng, ZHANG Yun-fang, NIE Zhao-hui, LIU Qiao-hong, ZHONG Jue. Effects of ultrasonic treatment on structure of roll casting aluminum strip [J]. Journal of

Central South University of Technology, 2007, 14(3): 363−369.

[17] ZHAO Jun, YU Kun, XUE Xin-ying, MAO Da-heng, LI Jian-ping. Effects of ultrasonic treatment on the tensile properties and microstructure of twin roll casting Mg−3%Al−1%Zn-0.8%Ce-0.3%Mn (wt.%) alloy strips [J]. Journal of Alloys and Compounds, 2011, 509(34): 8607−8613.

[18] LI Jian-ping, HU Jian-bing, MAO Da-heng, ZHAO Guan-zhong. Effects of ultrasound on the microstructures and mechanical properties of cast-rolling AZ31B magnesium alloy strip [J]. Materials Science Forum, 2011, 686: 129−134.

[19] JIANG Ju-fu, LIU Ying-ze, XIAO Guan-fei, WANG Ying, JU Ying-nan. Effect of pass reduction on microstructure, mechanical properties and texture of hot-rolled 7075 alloy [J]. Materials Characterization, 2019, 147: 324−339.

[20] FANG Hong-jie, LIU Hui, YAN Yang, LI Yun, XU Xiang-chun, CHU Xin, LU Yu-jiao, YU Kun. Microstructural and textural evolution of Al−4.5Mg−0.7Mn−0.2Sc alloys during hot rolling [J]. Materials Letters, 2021, 292: 129600.

[21] GASHTI S O, FATTAH-ALHOSSEINI A, MAZAHERI Y, KESHAVARZ M K. Effects of grain size and dislocation density on strain hardening behavior of ultrafine grained AA1050 processed by accumulative roll bonding [J]. Journal of Alloys and Compounds, 2016, 658: 854−861.

[22] FAN Wen-xue, BAI Yu, LI Guang-yang, CHANG Xing-yang, HAO Hai. Enhanced mechanical properties and formability of hot-rolled Mg−Zn−Mn alloy by Ca and Sm alloying [J]. Transactions of Nonferrous Metals Society of China, 2022, 32(4): 1119−1132.

[23] LIU Hai-ting, SHEN Yao, MA Jia-wei, ZHENG Peng-fei, ZHANG Lei. Grain size dependence of uniform elongation in single-phase FCC/BCC metals [J]. Journal of Materials Engineering and Performance, 2016, 25: 3599−3605.

[24] PRIYADARSHI A, KHAVARI M, SHAHRANI S B, SUBROTO T, YUSUF L A, CONTE M, PRENTICE P, PERICLEOUS K, ESKIN D, TZANAKIS I. In-situ observations and acoustic measurements upon fragmentation of free-floating intermetallics under ultrasonic cavitation in water [J]. Ultrasonics Sonochemistry, 2021, 80: 105820.

[25] SWALLOWE G M, FIELD J E, REES C S, DUCKWORTH A. A photographic study of the effect of ultrasound on solidification [J]. Acta Metallurgica, 1989, 37(3): 961−967.

[26] ESKIN D G, TZANAKIS I, WANG F, LEBON G S B, SUBROTO T, PERICLEOUS K, MI J. Fundamental studies of ultrasonic melt processing [J]. Ultrasonics Sonochemistry, 2019, 52: 455−467.

[27] ZHANG Yun, LI Rui-qing, LI Xiao-qian, YANG Yi-long, CHEN Ping-hu, DONG Fang, JIANG Ri-peng. Possible effects and mechanisms of ultrasonic cavitation on oxide inclusions during direct-chill casting of an Al alloy [J]. Metals, 2018, 8(10): 814.

[28] WANG Yi-chun, YAO Ming-chung. Realization of cavitation fields based on the acoustic resonance modes in an immersion-type sonochemical reactor [J]. Ultrasonics Sonochemistry, 2013, 20(1): 565−570.

[29] QIAN M, RAMIREZ A, DAS A. Ultrasonic refinement of magnesium by cavitation: clarifying the role of wall crystals [J]. Journal of Crystal Growth, 2009, 311(14): 3708−3715.

[30] STJOHN D H, EASTON M A, QIAN M, TAYLOR J A. Grain refinement of magnesium alloys: A review of recent research, theoretical developments, and their application [J]. Metallurgical and Materials Transactions A, 2013, 44: 2935−2949.

[31] HANSEN N. Hall−Petch relation and boundary strengthening [J]. Scripta Materialia, 2004, 51(8): 801−806.

[32] SHARMA V M J, KUMAR K S, RAO B N, PATHAK S D. Effect of microstructure and strength on the fracture behavior of AA2219 alloy [J]. Materials Science and Engineering: A, 2009, 502(1/2): 45−53.

[33] FADAVI BOOSTANI A, YAZDANI S, TAHERZADEH MOUSAVIAN R, TAHAMTAN S, AZARI KHOSROSHAHI R, WEI D, BRABAZON D, XU J Z, ZHANG X M, JIANG Z Y. Strengthening mechanisms of graphene sheets in aluminium matrix nanocomposites [J]. Materials & Design, 2015, 88(15): 983−989.

[34] BAILEY J E, HIRSCH P B. The dislocation distribution, flow stress, and stored energy in cold-worked polycrystalline silver [J]. The Philosophical Magazine: A Journal of Theoretical Experimental and Applied Physics, 1960, 5(53): 485−497.

[35] TRIVEDI P B, YASSAR R S, FIELD D P, ALLDREDGE R. Microstructural evolution and observed stress response during hot deformation of 5005 and 6022 Al alloys [J]. Materials Science and Engineering A, 2006, 425(1/2): 205−212.

[36] HANSEN N, HUANG Xiao-xu, UEJI R, TSUJI N. Structure and strength after large strain deformation [J]. Materials Science and Engineering A, 2004, 387: 191−194.

[37] HANSEN N. Boundary strengthening in undeformed and deformed polycrystals [J]. Materials Science and Engineering A, 2005, 409(1/2): 39−45.

[38] ZHAO Yong-hao, LIAO Xiao-zhou, JIN Zhe. Microstructures and mechanical properties of ultrafine grained 7075 Al alloy processed by ECAP and their evolutions during annealing [J]. Acta Materialia, 2004, 52(15): 4589−4599.

[39] PANTLEON W. Resolving the geometrically necessary dislocation content by conventional electron backscattering diffraction [J]. Scripta Materialia, 2008, 58(11): 994−997.

[40] RODGERS B I, PRANGNELL P B. Quantification of the influence of increased pre-stretching on microstructure-strength relationships in the Al−Cu−Li alloy AA2195 [J]. Acta Materialia, 2016, 108: 55−67.

[41] WANG Guan-gang, HUANG Guang-sheng, HUANG Yu, ZHANG Cheng, JIANG Bin, TANG Ai-tao, PAN Fu-sheng. Achieving high ductility in hot-rolled Mg−*x*Zn−0.2Ca−0.2Ce sheet by Zn addition [J]. JOM, 2020, 72: 1607−1618.

[42] YANG Cui-cui, LIU Zhi-wei, ZHENG Qiao-ling, CAO Yi-liang, DAI Xiao-han, SUN Liang, ZHAO Jing-rui, XING Jian-dong, HAN Qing-you. Ultrasound assisted in-situ casting technique for synthesizing small-sized blocky Al_3Ti particles reinforced A356 matrix composites with improved mechanical properties [J]. Journal of Alloys and Compounds, 2018, 747: 580−590.

超声辅助连铸连轧制造 1030B 铝板带的显微组织、力学性能和成形性能

张 莉[1]，李晓谦[2]，葛 尚[1]，黄 冠[1]，蒋日鹏[2]，谢敬佩[3]，关绍康[1]

1. 郑州大学 材料科学与工程学院 河南省先进轻合金重点实验室，郑州 450001；
2. 中南大学 轻合金研究院，长沙 410083；
3. 河南科技大学 材料科学与工程学院，洛阳 471003

摘 要：在 Hazelett 连铸连轧生产线上利用超声熔体处理改善了 1030B 铝板带的组织和性能。采用扫描电镜、电子背散射衍射仪和拉伸试验对合金的显微组织和性能进行表征。与未超声处理的常规样品相比，在超声作用下，铸板的平均晶粒尺寸减小了 28.0%以上，细小晶粒在轧板中也得以保留，轧板的平均晶粒尺寸小于 63.0 μm。同时，在轧制过程中，晶粒细化、动态回复和再结晶产生了较高的位错密度。因此，超声处理后轧态样品的应变硬化率普遍高于常规试样，轧板的强度也有所提高。而且，轧板具有较高的应变硬化指数和 Erichsen 指数，成形性较好。

关键词：晶粒细化；力学性能；成形性；连铸连轧；超声熔体处理；1030B 铝

(Edited by Xiang-qun LI)